Surface & Coatings Technology 335 (2018) 159–165

Contents lists available at ScienceDirect

Surface & Coatings Technology

journal homepage: www.elsevier.com/locate/surfcoat

Characterization of $Si_xO_yN_z$ coating on CF/PPS composites for space applications

Maria Paula de O.C. Cintra[a], Alberto L. Santos[a,*], Patrícia Silva[b], Mario Ueda[c], Andreas Janke[d], Dieter Jehnichen[d], Frank Simon[d], Edson C. Botelho[a]

[a] Materials and Technology Department, School of Engineering, Universidade Estadual Paulista (UNESP), Guaratinguetá, Brazil
[b] Associated Sensors Laboratory, INPE, São José dos Campos, Brazil
[c] Associated Plasma Laboratory, INPE, São José dos Campos, Brazil
[d] Leibniz Institute of Polymer Research, Germany

ARTICLE INFO

Keywords:
Advanced composites
Silicon oxynitride
Spatial environment
Plasma enhanced chemical vapor deposition
Plasma immersion ion implantation

ABSTRACT

This work deals with the processing and surface treatment of thermoplastic composites carbon fibers/Polyphenylene sulfide (CF/PPS) for aerospace applications. After the production of the thermoplastic composites through hot compression molding, a silicon deposition was carried out on its surface using Plasma Enhanced Chemical Vapor Deposition (PECVD). Then, the Plasma Immersion Ion Implantation (PIII) process was executed on the silicon coated samples to create an amorphous silicon nitride layer. Subsequently, the coated and uncoated samples were characterized by means of the following techniques: optical microscopy, atomic force microscopy (AFM), X-ray diffraction (XRD) and X-ray excited photoelectron spectroscopy (XPS). By analyzing all the results obtained from the characterizations, it was concluded that a layer of amorphous silicon oxynitride was generated on the CF/PPS composite without damaging it. This result is an innovative step concerning the application of this material in a space environment (low earth orbit).

1. Introduction

The great advantage of composite materials employment in practical applications is the possibility of obtaining products with different properties, such as: high elastic modulus, high mechanical resistance (tensile, compression, bending, etc.), low thermal conductivity, low specific weight and high ductility [1–3].

The composite materials were initially developed for the aerospace and military markets. This category of material offers superior structural performance compared to conventional metals. Nowadays, their application occurs in several fields, such as: aircraft, sports articles, heavy industry, oil and gas exploration and in the construction of wind turbines [4–8].

However, the main problem of the use of composites in the space industry is the difficulty of the material to withstand the spatial conditions, such as the attack of atomic oxygen, ultraviolet radiation, thermal cycling (− 150 °C to 150 °C) and high vacuum [9–11].

Concerning the vacuum resistance, the material must be stable, in order to cause minimal contamination by its volatiles of sensitive instruments. The composites exhibit large dimensional variations when the water is removed in the vacuum, which makes it difficult to use in such an environment. On the other hand, UV radiation is present throughout the spacecraft orbits, not changing the intensity with altitude, and can degrade most coatings (paint) and polymer films. The atomic oxygen attacks and erodes quickly the materials employed outside of space vehicles like thermal control revetments, paints and composite materials. In addition, thermal cycling may lead to the appearance of microcracks in composite materials, due mainly to differences in the thermal expansion coefficient [12].

To protect the composite from such conditions, many innovative studies about the surface treatment of these materials have been performed. Among these, silicon nitride film (Si_3N_4) is a good alternative to cover these composites [13,14]. Si_3N_4 is an advanced ceramic that stands out for its chemical and thermal stability, in addition to high hardness (around 22 GPa), low friction coefficient and good dielectric properties [15].

The surface of an engineering component is often subjected to wear and corrosion. The use of silicon nitride protective coatings mainly favors the industry where surface properties are of great importance. This coating increases the performance of cutting and forming tools against corrosion, wear and abrasion, thereby improving their physical chemical and mechanical properties [16]. Thus, silicon nitride is a good

* Corresponding author at: 333 Ariberto Pereira da Cunha Avenue, 12516-410, Guaratingueta, SP, Brazil.
E-mail address: santos.lima.alberto@gmail.com (A.L. Santos).

https://doi.org/10.1016/j.surfcoat.2017.12.036
Received 10 August 2017; Received in revised form 23 November 2017; Accepted 14 December 2017
Available online 15 December 2017
0257-8972/

candidate for coating tools used in high temperatures and other engineering components, because of their high hardness combined with thermodynamic stability and high temperature oxidation resistance [17,18]. Therefore, this material has an excellent potential to cover composite materials for use in the aerospace industry.

Plasma treatments are widely employed to modify the surface of several materials, since active species produced in the plasma can interact with the surface of materials in an efficient and economical manner [19]. In addition, they can produce modifications that could not be performed by conventional methods. To ensure that the composite is totally coated with a layer of silicon nitride, one possibility is to use previous deposition of silicon using the plasma enhanced chemical vapor deposition process (PECVD) followed by plasma immersion ion implantation (PIII) of nitrogen. The PIII process aims to improve the bonding of the Si_xO_y to the composite surface by recoil implantation of the film and homogeneous formation of $Si_xO_yN_z$. In this way, this work has as the main objective of processing the thermoplastic composites (CF/PPS) and its subsequent coating with a uniform layer of silicon nitride.

2. Experimental

2.1. Carbon fiber/Polyphenylene sulfide (CF/PPS) composites production

The carbon fibers used in this work were purchased from the HEXCEL Company in the form of plain weave fabric containing 3000 monofilaments per tow, with a specific mass of 1.77 g/cm^3. The PPS matrix was used as a 0.12 mm thick film. This film was purchased from Curbell Plastics, Largo-FL, USA. The matrix has a specific mass of 1.35 g/cm^3 and a melting temperature of about 285 °C.

The carbon fiber fabric and the PPS film were cut to dimensions of 200 mm × 200 mm and stacked to have a nominal volume ratio of 60% of CF in the final composite. A Carvel press, model CMG100H-15-0, was used to perform the hot compression molding of the CF/PPS composite. The Upilex® 25S, donated by UBE, Ube, Japan, was employed as solid release agent. The pressing parameters are shown in Table 1.

One plate was obtained after the processing, which was cut into 7 samples of approximately 60 mm × 60 mm. The 7 samples were separated as shown in Table 2.

2.2. CF/PPS composites coating

The silicon film on the CF/PPS composite was obtained from the plasma enhanced chemical vapor deposition (PECVD) technique, performed at the Associated Laboratory of Sensors and Materials (LAS) at the National Institute of Space Research (INPE), São José dos Campos, Brazil. The parameters used during this process are shown in Table 3.

Five samples (samples 3 to 7) with the silicon coating were subjected to the PIII process to obtain the silicon nitride layer. Nitrogen gas (N_2) was used in all treatments, however, the process parameters were varied for each sample, allowing a later comparison between the layers obtained. As the composite sample is dielectric, it was necessary to couple into a metallic net, in order to allow the ions acceleration from the plasma. The PIII process was carried out at the Plasma Associated Laboratory (LAP) at the National Institute of Space Research (INPE), São José dos Campos, Brazil. The parameters used in the PIII processes are shown in Table 4.

Table 1
Hot compression molding parameters.

Parameters	Variables
Temperature	340 °C
Pressure	1.5 MPa
Final composite dimensions	200 mm × 200 mm × 3 mm

Table 2
Description of the 7 composite samples.

Samples	1	2	3 to 7
Processing	–	PECVD	PECVD and PIII
Description/code	CF/PPS	CF/PPS + Si_xO_y	CF/PPS + $Si_xO_yN_z$

Table 3
Parameters used during the PECVD process.

Time	10 min
Work pressure	3.1×10^{-2} Torr
Source voltage	580 V
Source current	20 a 30 mA
Gas	Silane (SiH_4)

Table 4
Parameters used in the PIII process.

Sample	Time (min)	Working pressure (mbar)	Pulse frequency (kHz)	Pulse width (μs)	Pulse voltage (kV)	Current (A)
3	30	2.2×10^{-2}	1	30	1.5	1.0
4	15	2.4×10^{-2}	1	30	1.7	0.5
5	60	2.5×10^{-2}	1	30	1.8	0.4
6	30	5.0×10^{-2}	1	30	0.7	1.0
7	30	4.0×10^{-2}	1	30	1.5	1.0

2.3. Composites characterization

A Keyence optical microscope was used to compare non-coated samples with silicon and silicon nitride coated samples. AFM was performed in the scanning force microscope NanoScope IIIa-D3100 (Digital Instruments, USA) with the objective of measuring the thickness of silicon and silicon nitride layers in the coated samples. Adhesive tapes were attached to the samples and then removed. The difference in height between the surface of the film and the surface of the composite (area where the tape was taken off) indicated the thickness of the deposited film. The thicknesses of the layers were measured by AFM after the removal of adhesive strips in different regions of their surfaces.

XRD technique was applied on all samples in order to check the crystallinity of the silicon nitride layer on the surface of the composites. The experiment was carried out with the 2-circle X-ray diffractometer XRD 3003 T/T (GE Sensing & Inspection Technologies GmbH, Ahrensburg, Germany) in two different ways: WAXS (wide-angle X-ray scattering) - standard measurements in symmetric reflection (sample surface adjusted) and GIWAXS (grazing incidence WAXS) – with fix grazing angle 4° (surface illumination: ~10 × 7 mm^2) in asymmetric reflection.

XPS analysis was performed on all samples to determine the elements present on each composite. All XPS studies were performed using an ultra-high vacuum photoelectron spectrometer (Kratos Analytical). The spectrometer was equipped with an Al Kα ($h\cdot\nu$ = 1486.6 eV) with an X-ray source of 300 W up to 15 kV. The kinetic energy of the photoelectrons was determined with a hemispherical analyzer set to 160 eV for the scanning spectra and set to 20 eV to the high-resolution spectra. During all measurements, electrostatic charges of the sample were avoided by a low energy electron source, which worked in combination with a magnetic immersion lens. Subsequently, the C1s peak was set to 285.00 eV. High resolution spectra were deconvoluted using the Kratos deconvolution spectra software.

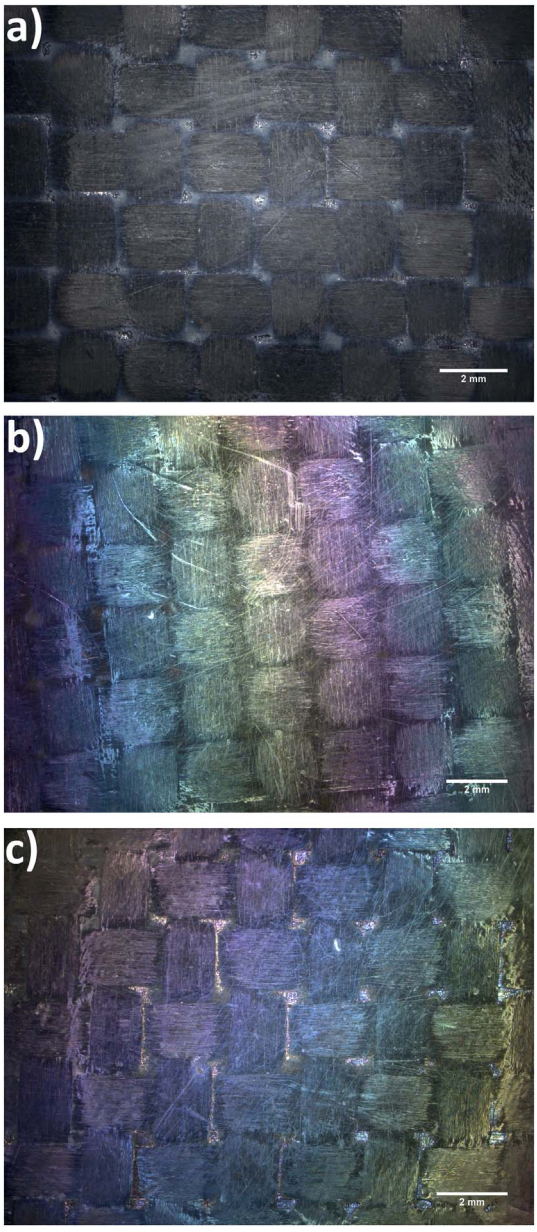

Fig. 1. CF/PPS composites surfaces, evaluated by optical microscopy: (a) without coating; (b) with silicon coating; and (c) with $Si_xO_yN_z$ coating (sample 6).

3. Results and discussion

3.1. Optical microscopy

The composites with and without coatings were characterized by optical microscopy for surface comparison. The images obtained during this characterization are presented in Fig. 1.

As can be observed in Fig. 1, the CF/PPS composite without coating (a) presents some voids on its surface (white dots between the weft and the warp). Such voids may impair the mechanical properties of the composite in its final application in spatial environment, since the fibers will be exposed.

Comparing the photos before and after the silicon film coating, it can be noticed that the film fills the voids present on the CF/PPS composites. Thus, it is concluded that the silicon film completely covered the sample of the composite and will prevent it from being exposed to the space environment. The difference in the shade observed on the coated samples surfaces was caused by the film layer thickness difference. This variation will be evaluated later through the AFM technique. Fig. 2 shows a region present in samples 3, 6 and 7.

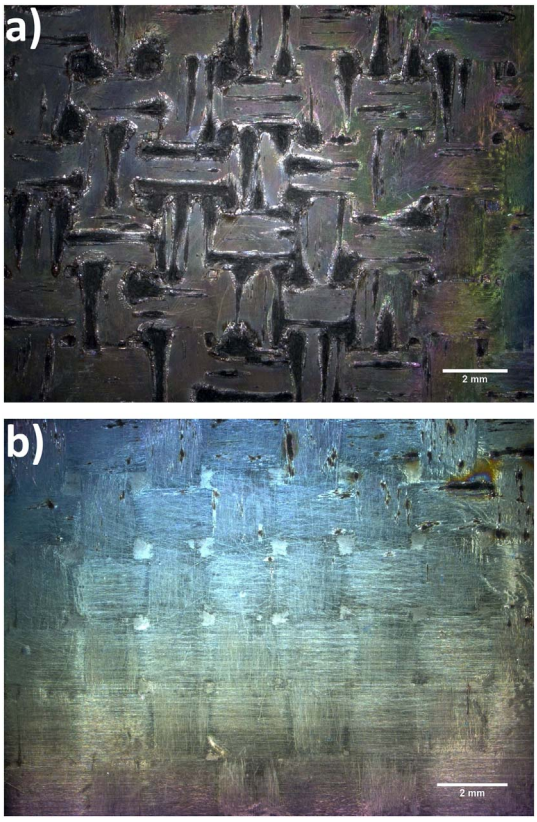

Fig. 2. Regions in samples (a) 3 and (b) 7, damaged by arc in PIII process.

In Fig. 2 it can be observed the presence of dark regions on the samples surfaces. These defects happen during the PIII process due to the occurrence of the electrics arcs. This phenomenon occurs due to the application of high voltage to a dielectric material. The composite accumulates electric charge, and this charge promotes the dielectric rupture of the matrix, causing the arcs. As the electric arc promotes the spot heating of the sample (where it occurs), small damages are entailed to the material. This problem can be solved by controlling better the PIII process (voltage and current).

3.2. Atomic force microscopy - AFM

The thicknesses of the layers were measured after the removal of adhesive strips in different regions of their surfaces, which allowed the visualization of the height difference between the layer and the removed part. Table 5 presents the measured values for the samples coated with silicon (2) and with $Si_xO_yN_z$ (4 and 5).

The total mean thickness of the layers was 275 ± 53 nm, this value is the thickness range expected for coatings using PECVD process [20]. A large standard deviation is observed, confirming the thickness variation observed in the optical microscopy (shadow difference).

Comparing the thickness of the silicon layer (sample 2) and the thickness of the silicon oxynitride layer, it can be observed that the $Si_xO_yN_z$ layer is thinner than the silicon layer. This fact can be explained by the sputtering phenomenon that occurred during the PIII

Table 5
Thickness values of the silicon and $Si_xO_yN_z$ layers measured by AFM.

Sample	2	4	5
Layer thickness (nm)	273 ± 67	135 ± 44	142 ± 49

process [21–25], which possibly eroded part of the existing silicon layer. Sputtering is inherent in the PIII process and can remove a lot of material form the substrate [22–25]. This process competes with the implantation process and is explained by the momentum transfer of accelerated plasma ions to the substrate atoms.

There may be doubt of where the delamination caused by the removal of the adhesive tape occurred. Whether it was caused at the composite/silicon film interface or between the region of the silicon film rich in nitrogen and the region poor in nitrogen.

Abramof et al. [26] implanted nitrogen ions on the surface of silicon. The pulse voltage was 12 kV (approximately 10 times greater than in this work) and the sample was heated (300 °C) to stimulate the diffusion. It was found a maximum modified depth of 80 nm. Beloto et al. [27] treated the surface of porous silicon by PIII, with 12 kV, and the modified depth was approximately 90 nm. Another study of implantation profile was made by Milési et al. [28], that treated solar cell devices with elevated temperatures (1000 °C), and observed a modified depth of 150 nm.

Thus, in this work, the modified depth of the silicon film should be inferior than 80 nm. As the measured thickness of the $Si_xO_yN_z$ film is approximately 140 nm, it can be inferred that the delamination caused by the tape was at the composite/film interface.

3.3. X-ray diffraction - XRD

XRD measurements were performed on the samples 1, 2, 4, 6 and 7 in two different ways: WAXS and GIWAXS. The result of this characterization is shown in Fig. 3.

Analyzing the results, it can be observed that the curves are very similar to each other, showing that the samples have a related solid state structure. The scattering curves were dominated by the two main reflections of orthorhombic PPS (2θ: ~18.9° (110) and ~20.6° (200/111)) as well as by a broad scattering maximum at 2θ ~ 25.5° as an intensity summation of the broadened (002) reflection of carbon fibers (meso-state) and further amorphous amounts of PPS and carbon [30]. It could not be observed any presence of crystalline structures of Si/SiO_2 (sample 2), and Si_3N_4 (samples 4, 6 and 7). However, it is possible that the samples have silicon/silicon oxide and silicon nitride in the amorphous form, which cannot be separated from the amorphous scattering amount definitely by XRD. On the other hand, these amounts should be low due to strong similarity in the scattering curves (including their amorphous parts) of all samples with applied surface layers (coatings).

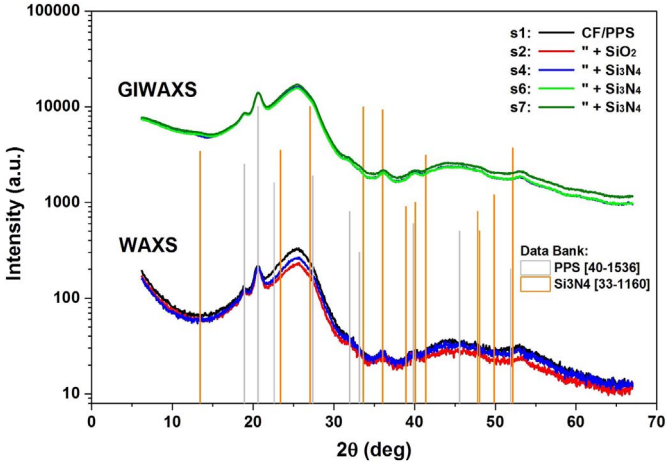

Fig. 3. Comparison of all samples measured with the two different X-ray methods, including reflection positions of PPS and Si_3N_4 [29].

3.4. X-ray photoelectrons microscopy – XPS

XPS analysis was performed in all samples to chemically analyze the surface of the CF/PPS composite. The following elements were found: carbon; nitrogen; oxygen; sulfur and silicon. And some contaminants: Sodium; aluminum; phosphor; chlorine; argon; potassium; calcium; chrome; iron; nickel and zinc. This contamination can be the result of auxiliary processes (chamber cleaning with argon) and the implantation of atoms from the PIII chamber itself, made of stainless steel, and from SS304 mesh. High resolution spectra were deconvoluted at component peaks with different binding energy values.

3.4.1. Carbon

The C1s spectra were obtained for all samples (Fig. 4) and then deconvoluted at five peaks (A, B, C, D and E). Comparing the spectra between them, it can be noticed that all spectra show a similar form.

Based on the binding energies found for the C1s peaks and literature values, it was possible to discuss the presence of the following carbon species. Peak A (285.00 eV) shows saturation of hydrocarbons. Peak B (285.66 eV) synthesizes the carbon atoms, which are bonded to the nitrogen (*C*—N) and carbon atoms located at the α position of carboxylic acid and methyl carboxylate ester groups (*C*—COO). The peak C (286.56 eV) represents the carbon atoms, which are involved in the C—O bonds, of alcohols (*C*—OH) and ethers (*C*—O—C). The carbon atoms of the alcohol alongside the carboxylate ester groups (O═C—O—*C*) also contribute to peak C. Peak D (287.11 eV) preferably shows the presence of aldehydes (H—*C*═O). The peak is small, because aldehydes can be easily oxidized. If there were amide groups present on the sample surface, peak D would also show the carbon atoms of the amide group (O═*C*—NH—C). The peak E (288.42 eV) is the resultant of the carbon atoms of the ester group (O═*C*—O—C). The carbon atom of the alcohol next to the ester group contributes to peak C.

3.4.2. Nitrogen

The N1s spectrum of sample 1 (Fig. 5) has a typical appearance of organic nitrogen bonds and was deconvoluted to 2 different peaks: K and L. Peak K (400.04 eV) shows the presence of nitrogen atoms bound to the amine groups (C—N) and/or amides (O═C—NH—C). Based on binding energy it is impossible to distinguish between primary, secondary and tertiary amine. But the intensity of peak B and the absence of component D (in the C 1s spectrum) confirm that there are preferably primary amines on the surface of sample 1. Peak L (402.63 eV) indicates the presence of the protonated amine group (C—N + H) and/or ammonium species. Slightly oxidized nitrogen (as N═O) could also contribute to the peak L (nitro, nitrite and nitrate groups have significantly higher binding energy values).

As can be observed in the N1s spectrum of sample 2 (Fig. 6), the deposition of silicon introduced a third peak J in the spectrum. The bonding energy value found is characteristic of silicon.

Samples 6 show a fourth peak, peak I (Fig. 7), which presented lower values of binding energy (396.27 eV). These binding energy values are observed for transition metal nitrides such as CrN. Bonding energies with values greater than 402.75 eV indicate the presence of oxidized nitrogen species.

3.4.3. Silicon

The Si2p spectrum of sample 1 (Fig. 8) is characterized by the unimodal distribution of Si2p photoelectrons (peak P at 102.37 eV). The binding energy value found (99.4 eV) is different from that found in the literature for the silicon binding state, which may be linked to possible contaminations by silicones (siloxanes) or by silica particles incorporated into the surface of the composite.

Plasma deposition of the silicon layer introduced different silicon species. The complexity of the Si2p spectrum required the deconvolution in 4 peaks (N, O, P and Q), as shown in Fig. 9.

Normally, the expected 2p3/2 peak expected for Si_3N_4 has a

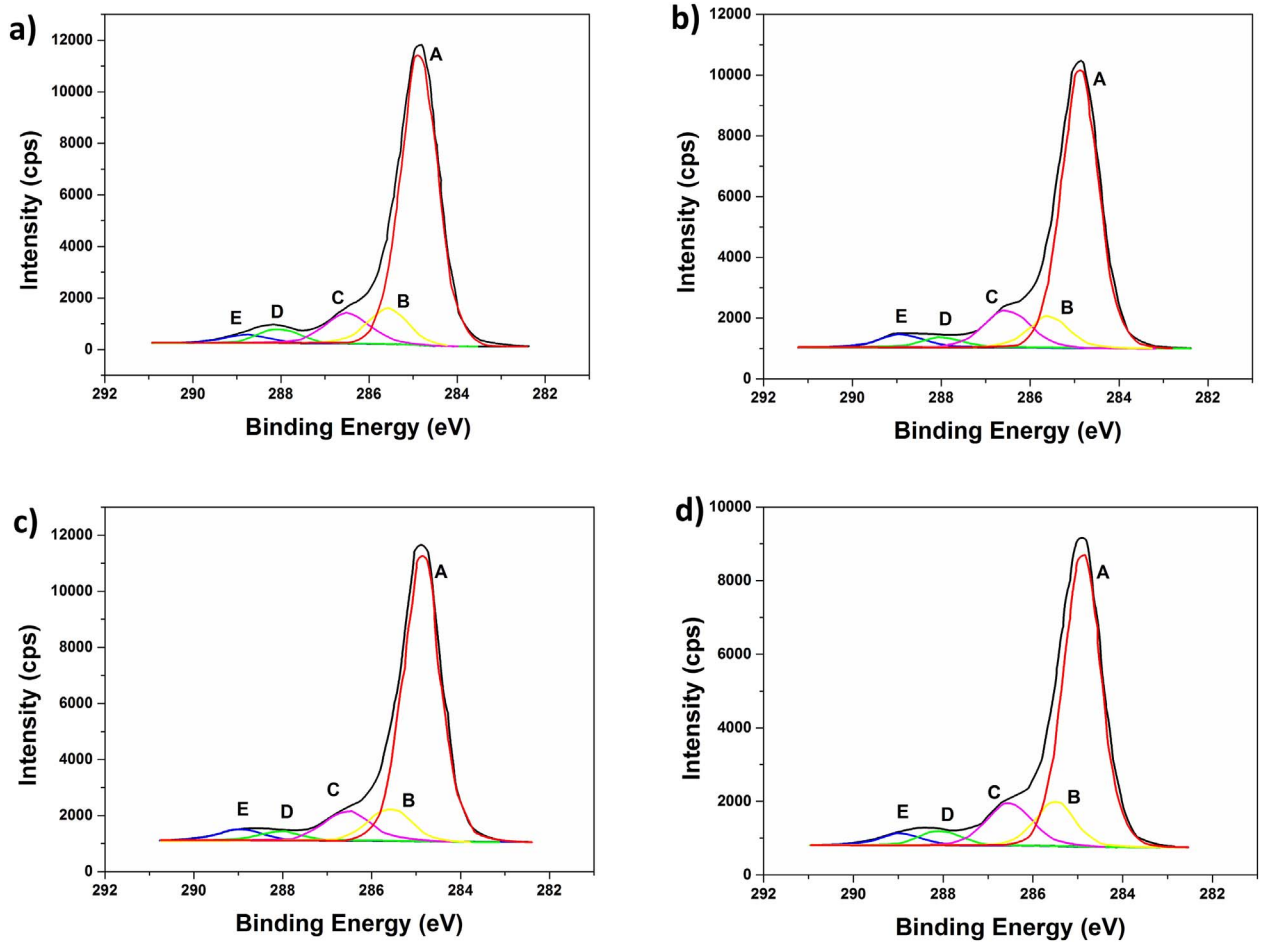

Fig. 4. C1s spectra of the CF/PPS composites surfaces: (a) without coating; (b) with silicon coating; and (c, d) with $Si_xO_yN_z$ coating.

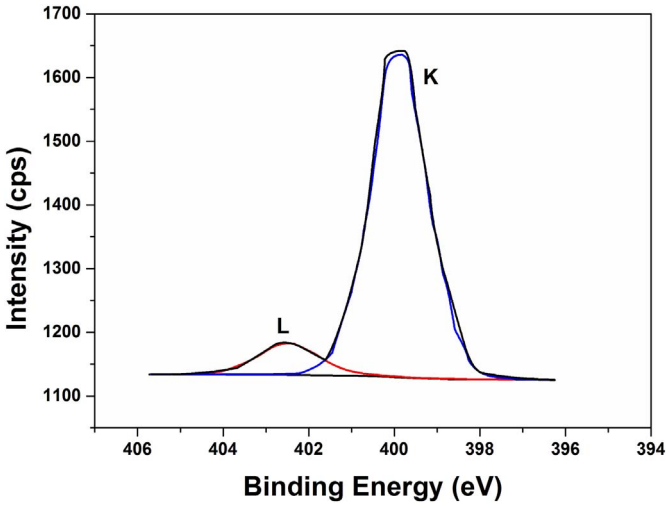

Fig. 5. Sample 1 N1s spectrum.

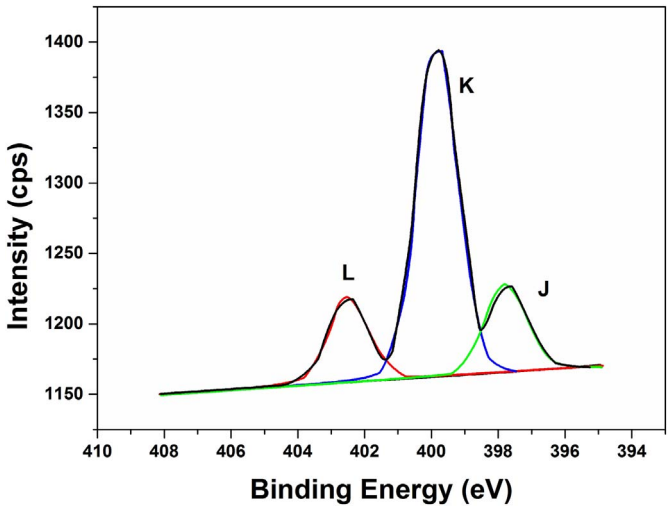

Fig. 6. Sample 2 N1s spectrum.

bonding energy of approximately 101.7 eV (N peak). It was possible to observe in Fig. 10 a well-defined peak with binding energy similar to that expected for Si_3N_4 (samples 4 and 5). This fact can be explained by the analysis of the parameters used in the PIII process, since for these two samples, higher voltage (1.7 and 1.8 kV) and lower current (0.4 and 0.5 A) were carried out, as shown in Table 4. The influence of the time 15 min, for sample 4, and 60 min, for sample 5, did not alter the Si_3N_4 peak. In other words, the ideal is to limit the PIII process to shorter time. Because this result shows that process of saturation occurs in a quite short time.

It is assumed that the deposition conditions did not allow the crystalline silicon to form, which corroborates the conclusion of the XRD analysis. All other Si2p peaks are likely to result from the oxidation of silicon species. Peak Q shows Si—OH groups, which are terminal groups typical of silicon oxide networks.

In general, it is concluded from the XPS analysis that the silicon layer is not crystalline and that it has been strongly oxidized in the form

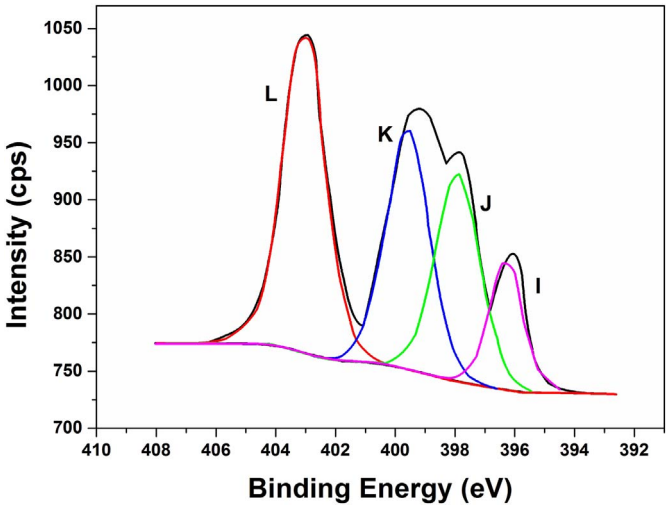

Fig. 7. Sample 6 N1s spectrum.

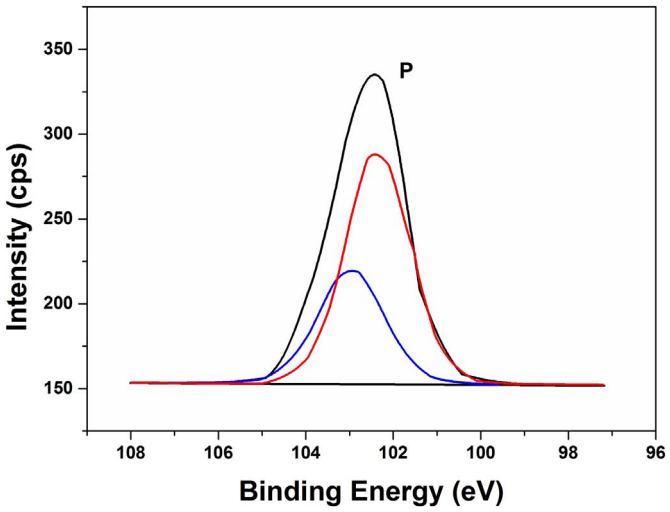

Fig. 8. Sample 1 Si 2p spectrum.

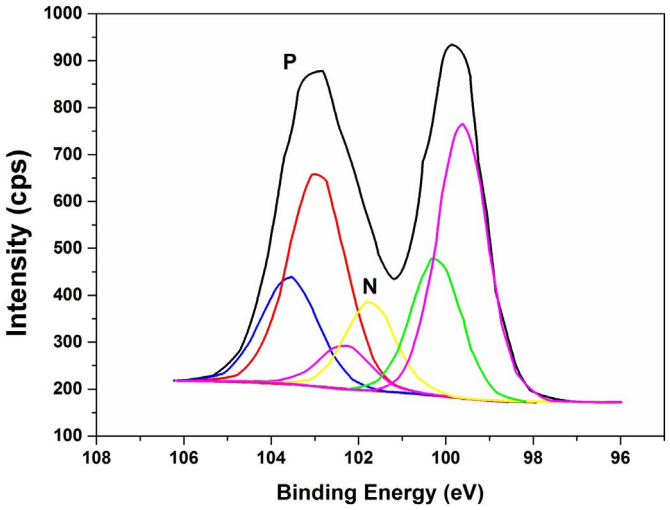

Fig. 9. Sample 2 Si 2p spectrum.

of various oxides but mostly in the form of SiO_2. Finally, the silicon nitride layer was not shown to be Si_3N_4 but $Si_xO_yN_z$, since silicon presented different forms of hybridization (Figs. 8–10).

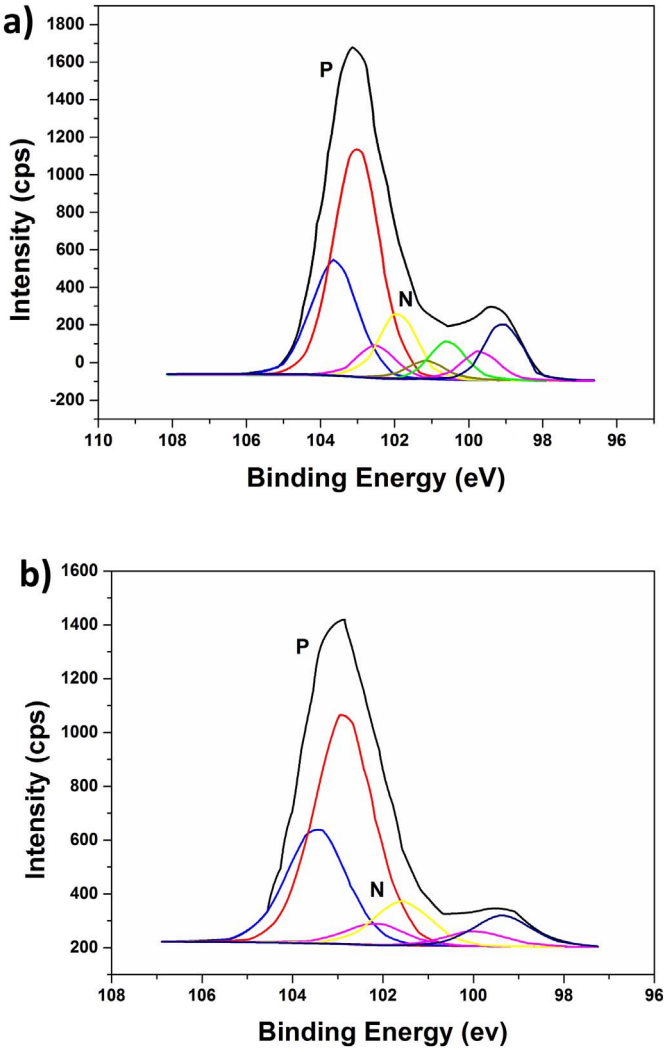

Fig. 10. Samples 4 and 5 Si 2p spectra.

Thus, the combination of the two plasma techniques (PECVD and PIII) presents a viable way of coating polymeric composites for their protection against atomic oxygen and maybe to other substances. Future work must be continued to investigate whether such $Si_xO_yN_z$ layer will efficiently protect the CF/PPS composite from the aggressive space environment.

4. Conclusions

After the processing of the CF/PPS composite by hot compression molding, subsequent coating with a layer of silicon through PECVD and PIII process, amorphous silicon oxynitride coated composites were obtained.

Some analyzes were carried out in order to characterize this layer. First, after the optical microscopy, it can be concluded that the silicon film completely covered the sample of the composite and will prevent it from being exposed to the space environment. Atomic force microscopy results showed that the thickness of the silicon nitride layer was 275 ± 53 nm. Future analyzes should be performed to assess whether this thickness is large enough to protect the composite from the space environment.

The results of the X-ray diffraction technique showed that there were no changes in the crystalline structure of the samples after the growth of the silicon nitride layer. On the other hand, results of the XPS analysis showed evidence of the presence of $Si_xO_yN_z$ (amorphous) in the

covered samples.

In general, after analyzing all the obtained results, it is concluded that through the two plasma assisted techniques (PECVD and IIIP), the initial objective of obtaining a layer of silicon nitride on a polymeric composite without damaging was achieved.

Acknowledgements

Thanks to Bernd Lauke and the Leibniz Institute of Polymer Research for allowing to become reality this work between Brazil and Germany. Thanks to FAPESP (2015/24915-3 & 2015/12154-8) and CNPq (303224/2016-9) for financial support.

References

[1] Carl Zweben, Advanced composite materials for optomechanical systems, Optomechanical Eng. SPIE Proc. 8836 (2013) 08.
[2] Qiang Liu, Xiyu Xu, Jingbo Ma, Jinsha Wang, Yu Shi, David Hui, Lateral crushing and bending responses of CFRP square tube filled with aluminum honeycomb, Compos. Part B 118 (2017) 104–115.
[3] Yin Li, Wei Zhang, An-Bo Ming, Zheng-Wei Yang, Gan Tian, A new way for revealing the damage evolution of impacted CFRP laminate under compression-compression fatigue load based on thermographic images, Compos. Struct. 176 (2017) 1–8.
[4] V.R. Leite, Estado da arte dos Materiais Compósitos na Indústria Aeronáutica, J. Exact Sci. 20 (2) (2014).
[5] David Delsart, Gérald Portemont, Mtthiaswaimer, Crash testing of a CFRP commercial aircraft sub-cargo fuselage section, Procedia Struct. Integr. 2 (2016) 2198–2205.
[6] Wen-Xue Wang, Terutake Matsubara, Junfeng Hu, Satoru Odahara, Tomoyuki Nagai, Takashi Karasutani, Yuji Ohya, Experimental investigation into the influence of the flanged diffuser on the dynamic behavior of CFRP blade of a shrouded wind turbine, Renew. Energy 78 (2015) 386–397.
[7] Himayat Ullah, Andy R. Harland, Vadim V. Silberschmidt, Dynamic bending behaviour of woven composites for sports products: experiments and damage analysis, Mater. Des. 88 (2015) 149–156.
[8] Rafea Dakhil Hussein, Dong Ruan, Guoxing Lu, Cutting and crushing of square aluminium/CFRP tubes, Compos. Struct. 171 (2017) 403–418.
[9] J.H. Han, C.G. Kim, Low earth orbit space environment simulation and its effects on graphite/epoxy composites, Compos. Struct. 72 (2006) 218–226.
[10] S.Y. Park, H.S. Choi, W.J. Choi, H. Kwon, Effect of vacuum thermal cyclic exposures on unidirectional carbon fiber/epoxy composites for low earth orbit space applications, Compos. Part B 43 (2012) 726–738.
[11] A.R. Hopkins, A.C. Labatete-Goeppinger, H. Kim, H.A. Katzman, Space survivability of carbon nanotube yarn material in low Earth orbit, Carbon 107 (2016) 77–86.
[12] Tianyu Liu, Quan Sun, Jieru Meng, Zhengqiang Pan, Yanzhen Tang, Degradation modeling of satellite thermal control coatings in a low earth orbit environment, Sol. Energy 139 (2016) 467–474.
[13] S. Qian-Qian, C. Xian-Hua, Friction and wear of rare earths modified carbon fibers filled PTFE composite under dry sliding condition, Appl. Surf. Sci. 253 (2007) 9000–9006.
[14] O.A. Lukianova, V.V. Sirota, Dielectric properties of silicon nitride ceramics produced by free sintering, Ceram. Int. 43 (2017) 8284–8288.
[15] Hosneara, Abul Hasnat, Abu Hasan Bhuyan, Structural and electrical properties of reaction bonded silicon nitride ceramics, Open Ceram. Sci. J. 2 (2012) 1–7.
[16] A.-K. Wolfrum, C. Quitzke, B. Matthey, M. Herrmann, A. Michaelis, Wear behavior of diamond-silicon nitride composites sintered with FAST/SPS, Wear, 2017.
[17] S. Hampshire, Silicon nitride ceramics – review of structure, processing and properties, J. Achiev. Mat. Manuf. Eng. 24 (1) (2007) 43–50.
[18] A. Ziegler, J.C. Idrobo, M.K. Cinibulk, C. Kisielowski, N.D. Browning, R.O. Ritchie, Interface structure and atomic bonding characteristics in silicon nitride ceramics, Science 306 (2004).
[19] S.F.M. Mariano, M. Ueda, R.M. Oliveira, E.J.D.M. Pillaca, N.M. Dos Santos, Magnetic-field enhanced plasma immersion ion implantation and deposition (PIII&D) of diamond-like carbon films inside tubes, Surf. Coat. Technol. 312 (2017) 47–54.
[20] M.I. Alayo, I. Pereyra, W.L. Scopel, M.C.A. Fantini, On the nitrogen and oxygen incorporation in plasma-enhanced chemical vapor deposition (PECVD) SiOxNy films, Thin Solid Films 402 (2002) 154–161.
[21] U. Kogelschatz, Dielectric barrier discharges: their history, discharge physics, and industrial applications, Plasma Chem. Plasma Process. 23 (1) (2003) 1–46.
[22] S.-M. Chen, J.M. Shannon, R.M. Gwilliam, B.Z. Sealy, Electrical characterization of silicon nitride produced by plasma immersion ion implantation, Surf. Coat. Technol. 93 (1997) 269–273.
[23] Satinder K. Sharma, Sumit Barthwal, Surface topography and morphology characterization of PIII irradiated silicon surface, Appl. Surf. Sci. 255 (2008) 2333–2337.
[24] M. Ueda, A.R. Silva, E.J.D.M. Pillaca, S.F.M. Mariano, J.O. Rossi, R.M. Oliveira, L. Pichon, H. Reuther, New possibilities of plasma immersion ion implantation (PIII) and deposition (PIII&D) in industrial components using metal tube fixtures, Surf. Coat. Technol. 312 (2017) 37–46.
[25] D. Manova, J. Lutz, S. Mändl, Sputtering effects during plasma immersion ion implantation of metals, Surf. Coat. Technol. 204 (2010) 2875–2880.
[26] E. Abramof, A.F. Beloto, M. Ueda, R. Günzel, H. Reuther, Reciprocal space mapping of silicon implanted with nitrogen by plasma ion implantation, Nucl. Inst. Methods Phys. Res. B 175-177 (2001) 229–234.
[27] A.F. Beloto, M. Ueda, E. Abramof, J.R. Senna, M.D. da Silva, C. Kuranaga, H. Reuther, A. Ferreira Da Silva, I. Pepe, Sponge-like and columnar porous silicon implanted with nitrogen by plasma immersion ion implantation (PIII), Surf. Coat. Technol. 156 (2002) 267–271.
[28] Frédéric Milési, Marianne Coig, Jean-François Lerat, Thibaut Desrues, Jérôme Le Perchec, Adeline Lanterne, Laurent Lachal, Frédéric Mazen, Homojunction silicon solar cells doping by ion implantation, Nucl. Inst. Methods Phys. Res. B 409 (2017) 53–59.
[29] Data Bank PDF-2, ICDD, Newtown Square, PA, USA, 2015.
[30] J.E. Spruiell, C.J. Janke, A Review of the Measurement and Development of Crystallinity and Its Relation to Properties in Neat Poly(Phenylene Sulfide) and Its Fiber Reinforced Composites. Report ORNL/TM-2004/304, Metals and Ceramics Division, Oak Ridge National Laboratory, Oak Ridge, TN, USA, (2004).